Decoherence of a matter wave by blackbody radiation

B. Décamps, A. Gauguet, J. Vigué, and M. Büchner*
Laboratoire Collisions Agrégats Réactivité, FeRMI, Université Toulouse III and CNRS UMR 5589, Toulouse, France

(Received 17 November 2017; accepted 3 April 2024; published 7 May 2024)

We have observed the decoherence of a lithium atomic wave during its propagation in the presence of the radiation emitted by tungsten-halogen lamps, i.e., decoherence induced by blackbody radiation. We used our atom interferometer to detect this decoherence by measuring the atom fringe-visibility loss. The absorption of a photon excites the atom, which spontaneously emits a fluorescence photon. The momenta of these two photons have random directions, and this random character is the main source of decoherence. All previous similar experiments used small-bandwidth coherent excitation by a laser, whereas incoherent radiation involves several technical and conceptual differences. Our approach is interesting as blackbody radiation is omnipresent and decoherence should be considered if particles resonant to electromagnetic fields are used.

DOI: 10.1103/PhysRevA.109.053306

I. INTRODUCTION

Decoherence of a quantum object results from its interaction with its environment, which then plays the role of a measurement device [1,2], i.e., both become entangled. In our experiment, the object is an atom, and the environment is a thermal photon bath. Experiments have tested this process for atoms, in particular for the coherence of a coupled motional state of trapped ions [3,4] and between discrete atomic levels [5] (for recent reviews see [6,7]).

The study of matter-wave decoherence can be done by interferometry. Various interferometry experiments have been performed such as the following:

(i) The decoherence of an atom wave arises from the absorption of a resonant photon, followed by the spontaneous emission of a fluorescence photon [8–12]. The absorbed photon is provided by a laser beam, and the decoherence is due to the fluorescence photon's random momentum, which induces a random phase shift.

(ii) The decoherence of a molecular wave describing the propagation of a fullerene molecule was induced by the emission of thermal radiation. In this experiment, the thermal radiation was enhanced by heating the molecules with a laser prior to their entrance in a Talbot-Lau interferometer [13].

(iii) The decoherence of an atom or molecular wave can also be induced by collisions with the gas in the vacuum chamber [14–16]. The momentum transferred by such a collision, considerably larger than that of a photon, has important consequences: an atom (or molecule) which collided may miss the detector with a non-negligible probability, while decoherence can be observed only if the atom (or molecule) is detected. This effect has been observed with heavy molecules in a Talbot-Lau interferometer [15,16] and with sodium atoms in a Mach-Zehnder interferometer using transmission gratings [14] and a moiré detection scheme [17]: in both cases, interference signals are observed with a wide detector.

We study here the decoherence due to propagation using blackbody radiation based on thermal light. Blackbody radiation interacts with any polarizable object through the ac Stark interaction. It shifts energy levels, and even at room temperature these shifts become relevant for atomic clocks [18].

A radiation gradient induces a force, as detailed by Sonnleitner *et al.* in the case of hydrogen atoms [19]. In 2018, Haslinger *et al.* measured this force using cold-cesium-atom interferometry [20]. This force does not play a relevant role in our atom-interferometry experiment as our setup minimizes radiation gradients. In our experiment, decoherence is induced by modification of the atom momentum due to photon scattering. A very large baseline atom interferometer such as the one cited by Canuel *et al.* [21] should set the temperature difference to below 0.1 K, thus reducing this effect.

II. OUR EXPERIMENTAL APPROACH

Our decoherence mechanism using thermal light radiation implies several differences from previous studies.

In the experiments using laser excitation [8–12,14], the laser beams were intense enough to saturate the resonance transition. The interaction time in the cited experiments is comparable to or shorter than the atom excited-state lifetime τ. In the saturation regime, this short time was sufficient to excite the atom at least once and to induce decoherence.

The radiation we use can be described as a blackbody radiation at a temperature T close to that of the lamp filament. The mean photon number per mode near the atom resonance frequency ω_r is very small, $\approx k_B T/(\hbar\omega_r) \ll 1$, so the excitation regime is very far from saturation. A long atom-radiation interaction time $t_{\rm int} \gg \tau$ is needed to produce a non-negligible excitation probability and an observable decoherence effect.

The radiation bath used is almost isotropic, leading to an isotropic random momentum exchange: each

*matthias.buchner@irsamc.ups-tlse.fr

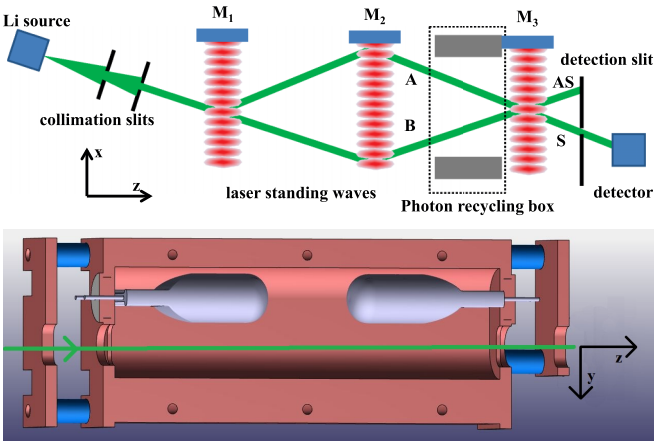

FIG. 1. Top: Schematic drawing of the atom interferometer (not to scale). The photon-recycling box is placed before the third mirror. Bottom: Open view of the photon-recycling box: two tungsten-halogen lamps are located inside the box, with their axis 10 mm above the atom-interferometer arms. The box is made of copper, with a silver coating on its internal surface. Light baffles at the two ends of the box reduce the power radiated directly toward the support of the laser standing-wave mirrors M_i. The box is cooled by water flowing in copper pipes (not represented).

absorption-emission process involves the transfer of two random photon momenta.

Decoherence experiments are frequently discussed as being experimental realizations of Heisenberg's microscope Gedankenexperiment [22,23]. Laser light shines on the interferometer arms, and if the arm separation is smaller than approximately half of the exciting laser wavelength, the detection of a scattered photon cannot reveal the spatial position of the scattering atom with sufficient precision to distinguish on which interferometer path the atom emitted the photon. The which-path information cannot be revealed, and high-contrast interferences can be observed [1,11]. If the separation is larger, the ability to discriminate the which-path information exists in principle, and this information may be extracted by a measurement of the emitted photon. In our experiment, the arm separation is several orders of magnitude larger than the 671-nm blackbody radiation.

We use isotropic blackbody radiation. Scattered photons are embedded into the blackbody photons, and a Heisenberg detector cannot distinguish them. Using our experimental parameters and assuming the characteristics of a Heisenberg photon counter, we estimate the contribution of a one-photon scattering toward a hypothetical photon counter (see Appendix A for details). At 2300 K, we find a mean photon number of the blackbody radiation of $\overline{n}_{\mathrm{BB}} = 8086.6$. If we take $\overline{n}_{\mathrm{BB}} + 1$ counting events, we find that the ratio of a scattered and detected photon is less than 1%.

III. THE EXPERIMENTAL SETUP

Our experiment (see Fig. 1) is based on a Mach-Zehnder atom interferometer [24]. A lithium atomic beam is produced by supersonic expansion of a lithium-argon mixture, with mean lithium velocity $u \approx 1055\ \mathrm{m\,s^{-1}}$, corresponding to a de Broglie wavelength $\lambda_{\mathrm{dB}} \approx 53$ pm for ^{7}Li.

Bragg atom diffraction by quasiresonant laser standing waves is used to split, reflect, and recombine the atom wave. The wavelength of the laser used for the laser diffraction is about $\lambda_r = 671$ nm, with its frequency shifted ≈2 GHz to the blue side of the D_2 resonance line of ^{7}Li. At this laser wavelength, only this isotope contributes to the interferometer signal.

A 50-μm-wide detection slit, located 400 mm after the third laser standing wave, selects one of the interferometer output beams which is detected by a Langmuir-Taylor hot-wire detector. The signal intensity $\mathcal{I}$ can be described by

$$\mathcal{I} = \mathcal{I}_0[1 + \mathcal{V}_0 \cos\varphi_d], \tag{1}$$

where $\mathcal{I}_0$ is the mean intensity and $\mathcal{V}_0$ is the fringe visibility, with typical values of $\mathcal{I}_0 \approx 3 \times 10^4$ detected atoms per second and $\mathcal{V}_0 \approx 70\%$. The phase φ_d, which is sensitive to the position of the mirrors M_i forming the laser standing waves, is used to scan the interference fringes by displacing mirror M_3.

Decoherence will be observed if (1) an atom crossing the interaction region has a large excitation probability, (2) the transferred momentum is sufficient to randomize the atom wave phase, and (3) an atom which experienced a scattering event can be detected. Let us discuss these three conditions.

(i) In the presence of blackbody radiation, the normalized populations P_g and P_e of the ground and excited states are in equilibrium with the radiation:

$$\frac{P_e}{P_g} = \frac{g_e}{g_g} \exp\left[-\frac{\hbar\omega_r}{k_B T}\right], \tag{2}$$

where g_g and g_e are the degeneracies of states g and e. For this equilibrium situation, the excitation rate γ_{exc} is equal to the rate of spontaneous emission P_e/τ, given by

$$\gamma_{\mathrm{exc}} = \frac{P_e}{\tau} \approx \frac{g_e}{g_g \tau} \exp\left[-\frac{\hbar\omega_r}{k_B T}\right] \tag{3}$$

using $P_g \approx 1$. For a lithium atom the ground state is ^2S, and ^2P is the first resonant state; $g_e/g_g = 3$, $\hbar\omega_r/k_B = 21443$ K, and $\tau = 27.1$ ns. An excitation rate $\gamma_{\mathrm{exc}} = 1 \times 10^4\ \mathrm{s^{-1}}$ is reached for $T \approx 2300$ K, and decoherence can then be observed with an interaction time $t_{\mathrm{int}} \approx \gamma_{\mathrm{exc}}^{-1} \approx 100\ \mu\mathrm{s}$.

The photon number volumetric density at ω_r inside a fully closed blackbody box, ρ_N, is given by Planck's law. We used a photon-recycling box in the interaction region which is not fully closed, and the walls are not perfectly reflective at ω_r. Consequently, ρ_N is reduced by a dilution factor $D(\omega_r)$. Using Eq. (3), we have

$$D(\omega_r)\rho_N(T) = D(\omega_r)\frac{8\omega_r^2}{\pi^2 c^3}\frac{1}{\exp\left(\frac{\hbar\omega_r}{k_B T}\right) - 1}\Delta\omega$$

$$\approx \frac{8\omega_r^2}{3\pi^2 c^3} D(\omega_r)\gamma_{\mathrm{exc}}\tau\,\Delta\omega, \tag{4}$$

with $\Delta\omega$ being the frequency interval of interest. The approximation holds for $\hbar\omega_r \gg kT$, which is valid in our experiment. The effective excitation rate is thus given by $D(\omega_r)\gamma_{\mathrm{exc}}$. In Appendix B we estimate $D(\omega_r)$, but we use a fit of our model to the experimental results to determine the effective $D(\omega_r)$.

(ii) The transferred momentum $\hbar\Delta k_x$ is the sum of the random and isotropically distributed momenta of two photons.

The transferred momentum probability distribution $P^{(\Delta)}(\Delta k_x)$ can be easily calculated if the two photon momenta are random and uncorrelated: this is exact if one averages over all the ground-state hyperfine Zeeman sublevels. Following the discussion by Chapman *et al.* [11] and Pritchard [1], the phase shift due to this event is equal to $\Delta\varphi = \Delta k_x d_x$, where d_x is the distance between the two interferometer arms at the point where the absorption-emission cycle occurs.

In our experiment, the center of the interaction region is placed at $\Delta z_{pb} = 80$ mm before the center of the third laser standing wave, and the interferometer-arm separation d_x reads $d_x = (2\lambda_{\rm dB}/\lambda_r)\Delta z_{pb} = 12.9$ μm. As d_x is large against λ_r, the interference term in Eq. (1), $\cos(\varphi_d + \Delta k_x d_x)$, oscillates rapidly with Δk_x, and the fringe signal averaged over $P^{(\Delta)}(\Delta k_x)$ is fully washed out, as explained in Sec. IV.

More sophisticated calculations involving the Wigner function were developed by Hornberger *et al.* [25] to describe decoherence of fullerene molecules inside a Talbot-Lau interferometer [13,15,16]. This formalism can be applied to our experiment, but the necessary modifications are out of the scope of the present paper.

(iii) An absorption-emission cycle changes the atom momentum and its probability of reaching the detector. This effect increases with the distance between the photon-scattering event and the detection slit. In order to minimize the atom-loss probability, we placed the interaction region as close as possible to the detection slit. With an interaction region length $l_{\rm int} = 100$ mm, the mean interaction time is $t_{\rm int} \approx 94\,\mu{\rm s} \approx 3400\tau$.

Blackbody radiation is usually produced inside an almost closed oven heated at temperature T. However, reaching a temperature of $T \sim 2300$ K is challenging, and the required power, several kilowatts, would perturb the very sensitive alignment of the interferometer [24]. To minimize the heat transferred to the interferometer, we chose to use two tungsten-halogen lamps placed above the atom trajectories inside a copper water-cooled box (see Fig. 1).

We used 5-mm-wide slits at the entrance and exit of the box, so that even with a rough alignment, the two interferometer arms cross easily this box. Wide slits also enhance the pumping speed of the box and reduce any pressure increase in the box due to outgassing induced by the lamps.

The internal walls of the box are coated with silver because this metal has the largest reflection coefficient, ≈ 99%, at the lithium resonance frequency ω_r. To evaluate the spectral energy density inside the box at this wavelength, we must know the lamp filament temperature T as a function of the lamp current I and the dilution factor $D(\omega_r)$, which is defined by the density of radiation energy as a fraction of the blackbody radiation.

We explain in Appendixes B and C how we proceeded. The current supply for the lamps might create a magnetic gradient which decreases fringe visibility. We estimated its contribution and found it to be negligible (see Appendix D for details).

For a current I in the 7–12-A range, the filament temperature T is given by $T \approx 765.6 \times I^{0.611}$ (K). The dilution factor $D(\omega_r)$, deduced from a thermodynamic model, is $D(\omega_r) \approx 17\%$ for a clean silver surface. Unfortunately, after operation of the lamps under vacuum, the box's internal surface was covered by a thin layer of black soot due to the cracking of the vapor of the Santovac oil used in the diffusion pumps by the UV radiation of the lamps. This soot layer considerably increased the probability of photon absorption by the box walls and reduced $D(\omega_r)$ to close to $1.4\% \pm 0.1\%$, a value deduced from a fit of the measured decoherence. This value corresponds to a diffuse reflection coefficient of ≈45%.

As the halogen lamps are placed above the interferometer arms, the light pressure may differ in the vertical (y) directions, which would break the isotropic symmetry. However, the vertical (y) acceptance of the detection slit is large; its effective width is about 1 mm, not causing any atom losses. The homogeneity of the atom momentum transfer in the horizontal (x) direction due to absorption-emission cycles is not affected.

IV. OUR MODEL

The absorption cycles change the atom momentum by $\hbar\Delta\mathbf{k}$; i.e., all directions are concerned as the blackbody radiation is almost isotropic. As the detection slit is about 1 mm large in the vertical direction (y axis), all deviating atoms in this direction are detected, and we drop this coordinate.

After one absorption and emission of a photon, the atom decays by spontaneous emission into the electronic ground state, but the magnetic hyperfine sublevel may be changed. If the incoming photon has a momentum along the z coordinate, the excitation does not occur on the same z coordinate for the two interferometer arms. The distances along the interferometer arms traveled by the atom in the new hyperfine sublevel are different. In our experimental setup, we have a weak nonzero homogenous magnetic field, and the Zeeman effect introduces a phase shift. We show in Appendix E that this phase shift is negligible. Therefore, we assume that the k_z component of the atom momentum change does not influence the interferometer signal.

Before detailing our model to describe the effect of radiation on the interferometer signal, we resume the main results. Let P_n be the probability for an atom to follow n absorption-emission cycles during the interaction time $t_{\rm int}$. We will show that, as soon as $n > 0$, the atom loses its phase coherence. It contributes to the phase-insensitive part of the interference signal with a probability π_n.

We set π_0 to unity. For $n > 0$, π_n is a function of the geometry of the interference arms and the detection-slit width. The probability P_n of n absorption-emission cycles is given by a Poisson distribution:

$$P_n(\gamma_{\rm exc}) = \frac{(\gamma_{\rm exc} t_{\rm int})^n}{n!}\exp(-\gamma_{\rm exc} t_{\rm int}), \tag{5}$$

$\gamma_{\rm exc}$ is assumed to be constant but will be adjusted to take into account the dilution factor D. We will show that the effect of the radiation on the fringe intensity $\mathcal{I}_0$ and visibility $\mathcal{V}_0$ is given by

$$\mathcal{I}_{0,\rm rel} = \sum_{n=0}^{\infty} P_n(\gamma_{\rm exc})\,\pi_n/\pi_0,$$
$$\mathcal{V}_{0,\rm rel} = \frac{P_0(\gamma_{\rm exc})\,\pi_0}{\sum_{n=0}^{\infty} P_n(\gamma_{\rm exc})\,\pi_n}. \tag{6}$$

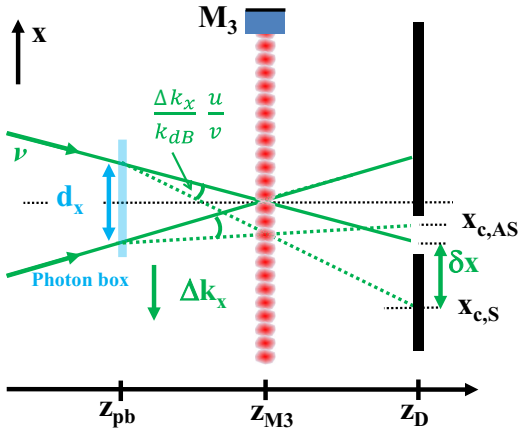

FIG. 2. Due to absorption-emission cycles, atoms receive an additional momentum $\hbar\Delta k_x$ and are deviated by the angle $(\Delta k_x/k_{\rm dB})(u/v)$.

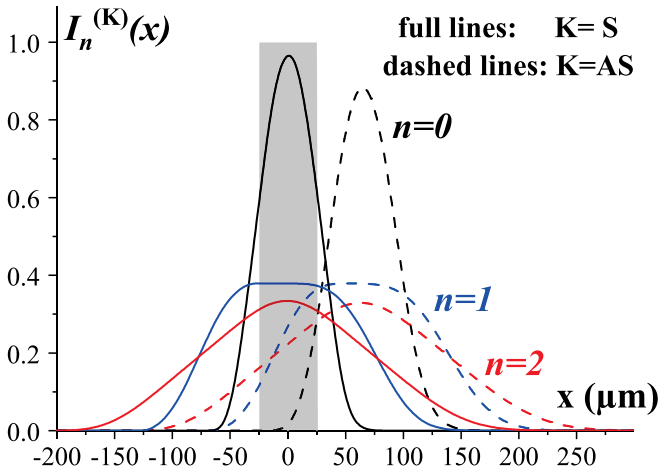

FIG. 3. The intensity profiles $I_n^{(K)}(x)$ ($K = $ S, AS) are traced for $n = 0, 1, 2$. The solid lines represent the symmetric outputs ($K =$ S), and the dashed lines indicate the antisymmetric ones ($K =$ AS). The detection slit, centered at $x = 0$, with a width of $w = 50$ μm is represented as a gray shaded rectangle.

$\mathcal{I}_{0,\rm rel}$ and $\mathcal{V}_{0,\rm rel}$ are the relative values. They are very sensitive to the values of π_n, as shown by two extreme cases:

(i) If $\pi_n = 1$ for all n, i.e., there are no atom losses, $\mathcal{I}_{0,\rm rel} = 1$, and $\mathcal{V}_{0,\rm rel} = P_0 = \exp[-\gamma_{\rm exc} t_{\rm int}]$.

(ii) If $\pi_n = 0$ for all $n > 0$, i.e., all excited atoms are lost, $\mathcal{I}_{0,\rm rel} = \exp[-\gamma_{\rm exc} t_{\rm int}]$, and $\mathcal{V}_{0,\rm rel} = 1$.

We now present our model in more detail. We analyze the effect of radiation on the atom beams, which contain the symmetric (S) and antisymmetric (AS) interferometer signals (see Fig. 1). All other stray beams have negligible intensities [24].

Following the approach of [11], the n absorption-emission cycles change the atom momentum by $\hbar\Delta\mathbf{k}$ and the atom wave phase by $\Delta k_x d_x$.

Along the horizontal (x) direction, the atom wave deviates by an angle $(\Delta k_x/k_{db})(u/v)$, with $k_{db} = 2\pi/\lambda_{\rm dB}$ being the de Broglie wave-vector amplitude at the atom mean velocity $u = 1055$ m s^{-1} and v being the atom velocity. Following Fig. 2, the displacement δx on the detector-slit plane reads

$$\delta x = \frac{\Delta k_x}{k_{\rm dB}} \frac{u}{v} (z_D - z_{M3} + z_{\rm ph}), \tag{7}$$

with z_D and z_{M3} being the positions of the detector slit and $z_{\rm ph}$ being the position of the absorption-emission cycle.

The center positions of the symmetric and antisymmetric atom beams on the detector plane are given by

$$\begin{aligned} x_{c,\rm S}(v) &= \delta x + \theta_B \frac{u}{v}(z_{M2} - z_{M1}), \\ x_{c,\rm aS}(v) &= \delta x + \theta_B \frac{u}{v}(z_D - z_{M2}). \end{aligned} \tag{8}$$

with $\theta_B = k_L/k_{\rm dB} \approx 80.5$ μrad being the first-order Bragg angle for atoms at the mean velocity u and k_L being the wave-vector amplitude for the standing-wave laser.

$P_n^{(\Delta)}(\Delta k_x)$ is defined as the probability density function for n-cycle, Δk_x momentum transfer. This function is evaluated in Appendix F. In the experiment of Chapman *et al.* [11] and in ours, no information about Δk_x is available, and we have to integrate over this quantity. The atom flux intensity at the detection-slit plane at z_D is given by the sum of the S and AS output beams of the interferometer. Both are composed of the sum over n of $P_n^{(\Delta)}(\Delta k_x)$ weighted by the Poisson probability $P_n(\gamma_{\rm exc})$:

$$I(x) = \sum_{n=0}^{\infty} P_n(\gamma_{\rm exc}) \left[I_n^{(\rm S)}(x) + I_n^{(\rm AS)}(x) \right], \tag{9}$$

with

$$\begin{aligned} I_n^K(x) = \int_0^\infty \int_{-\infty}^\infty & P_n^{(\Delta)}(\Delta k_x) P(v) I_0(x - x_{c,K}) \\ & \times \left[1 \pm \mathcal{V}_0 \cos\left(\theta_d + \Delta k_x d_x(v) \frac{u}{v} \right) \right] d\Delta k_x dv, \end{aligned}$$

where $K =$ S, AS denotes the contribution of the symmetric and antisymmetric output ports of the interferometer. The plus (minus) sign before $\mathcal{V}_0$ should be used for $K =$ S ($K =$ AS). $I_0(x)$ is the intensity, and $P(v)$ is the velocity profile of the nondiffracted atom beam. In our experiment $P(v)$ is well described by a Gaussian distribution:

$$P(v) = \frac{S_{||}}{u\pi} \exp\left[-\left(\frac{(v-u)S_{||}}{u} \right)^2 \right], \tag{10}$$

with $S_{||} \approx 8$ being the longitudinal velocity ratio. $I_0(x)$ can be modeled by a trapezoidal shape using the collimation-slit geometry. The top width is given by the collimating-slit width $w_S = 18$ μm (S_0 and S_1; see Fig. 1). The bottom width is 99 μm.

Finally, we numerically calculate the detector signal. We confirmed that for $n > 0$ the terms involving the cosine are negligibly small (e.g., for $0 < n \leqslant 3$, the correction is $< 10^{-4}$).

Figure 3 shows the results for $I_n^{(\rm S)}(x)$ and $I_n^{(\rm S)}(x)$ for $n = 0, 1, 2$. The shaded region represents the detection slit with a width of $w = 50$ μm, which selects the interferometer outputs.

The photon absorption-emission process increases the momentum width of the atoms; i.e., it broadens the beams, thus resulting in losses for the symmetric beam or a gain due to the

TABLE I. The relative signals and the probabilities π_n calculated by numerical integration.

n	$S_n^{(S)}$	$S_n^{(AS)}$	π_n
0	0.93	0.07	1.00
1	0.40	0.26	0.66
2	0.35	0.24	0.59
3	0.29	0.23	0.52

antisymmetric beam. We define the relative signals $S_n(K)$, and we deduce the probabilities π_n:

$$S_n^{(K)} = \int_{-w/2}^{w/2} I_n^{(K)}(x)dx,$$
$$\pi_n = \frac{S_n^{(S)} + S_n^{(AS)}}{S_0^{(S)} + S_0^{(AS)}}. \quad (11)$$

A numerical integration provides the values of π_n used in Eq. (6), as summarized in Table I.

We use our model to fit the experimental results. The only fitted parameter is the dilution factor D, which modifies the excitation parameter γ_{exc} (see Appendix B). Only the probabilities for the absorption-emission cycles $P_n(\gamma_{exc})$ are affected, while the probabilities π_n are independent of this parameter. The results from this model and our experimental results are plotted in Fig. 4.

V. EXPERIMENT AND RESULTS

In the first step, we outgassed the box walls by running the lamps at a moderate power without water cooling. Then, with water cooling on, we tested the effect of the lamps on the interferometer alignment: using an electronic autocollimator (LDS-Vector, Newport) to measure the orientation of mirror

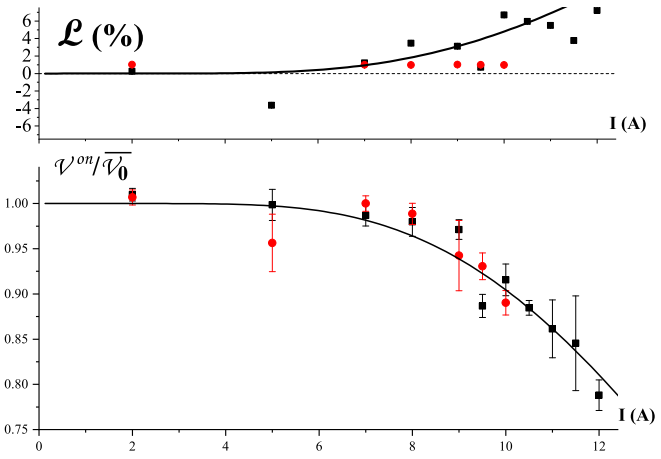

FIG. 4. Plot of the relative values of the mean intensity loss $\mathcal{L}(I)$ and relative visibility as a function of the current I sent through the lamps. The data points are experimental, while the solid curves represent the results of the model, using a fit for the visibility. We use our model with the calculated values $\pi_1 = 0.66$, $\pi_2 = 0.59$, and $\pi_3 = 0.52$. The dilution factor is obtained by fitting the experimental data for the visibility, and we get $D(\omega_r) = 1.4\% \pm 0.1\%$.

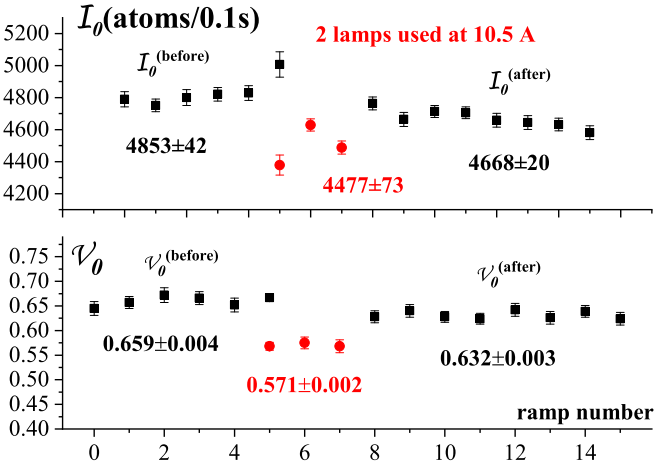

FIG. 5. We scan the interference fringes and extract the visibility and the mean signal. The black squares represent the values in the absence of the blackbody radiation. The red circles represent the values with the two lamps lit up at 10.5 A.

M_3, we measured that its orientation drifts up to ~300 μrad after a few minutes with the lamps on.

As the interferometer requires a mirror orientation within ±5 μrad of its optimum value, we cannot continuously run the lamps. We chose to alternate on-off periods with respective durations of 20 and 600 s. During a 20-s on period, the energy transferred to the mirror support is small enough to induce only a very small misalignment which relaxes during the 600-s off period. In order to measure the mean intensity and the visibility we use the same procedure developed in our previous experiments (see, e.g., [26]). We vary the phase φ_d [Eq. (1)] by ramping the x position of mirror M_3 (Fig. 1).

We record the fringe signal before, during, and after the lamp-on period, and we measure the fringe mean intensity $\mathcal{I}_0$ and the fringe visibility $\mathcal{V}_0$ in these three case; the thermal transient of the lamps, about 1 s, is discarded from the analysis.

Figure 5 shows one result for the fringe intensity and visibility. At the beginning the two lamps are switched off; we light them by applying a current of 10.5 A, and then, they are switched off. The lamp-on data, represented by red circles, are taken between the two lamp-off measurement sets, represented by black squares. The effect is clearly visible for both quantities.

We compare the fringe intensity and visibility during the on period to the corresponding values for the off period, defined as the mean of the values measured just before and after the lamp-on period: $\bar{\mathcal{I}}_0 = (\mathcal{I}_0^{(before)} + \mathcal{I}_0^{(after)})/2$ and $\bar{\mathcal{V}}_0 = (\mathcal{V}_0^{(before)} + \mathcal{V}_0^{(after)})/2$.

Figure 4 presents the plots of the mean intensity loss $\mathcal{L}(I) = 1 - \mathcal{I}_0^{on}(I)/\bar{\mathcal{I}}_0$ and the relative visibility $\mathcal{V}^{on}(I)/\bar{\mathcal{V}}_0$ as a function of the current I circulating in the lamps. The lines are the results of our model using Eqs. (6). We used the calculated probabilities π_n ($n = 0, \ldots, 3$), listed in Table I and the absorption-emission-cycle probabilities $P_n(D\gamma_{exc})$ with the dilution factor D as the only fit parameter for the relative fringe visibility. We found $D = (1.4 \pm 0.1) \times 10^{-2}$.

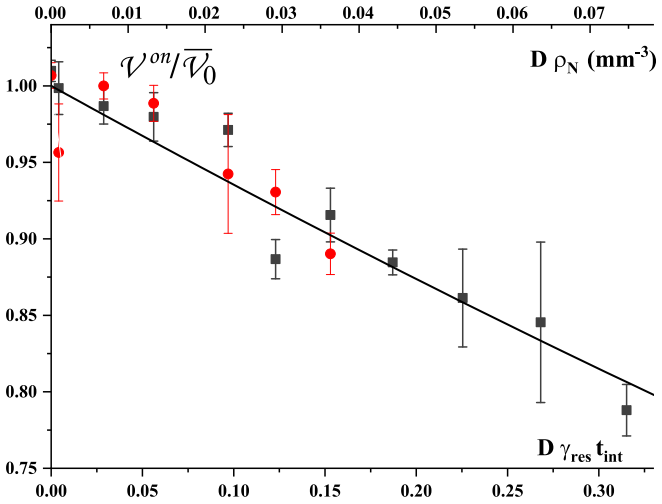

FIG. 6. The relative visibility plotted as a function of $D\gamma_{\rm exc}t_{\rm int}$. The data points are experimental, while the solid line represents the results of our model. The upper x axis shows the photon number density $D\rho_N$ emitted by blackbody radiation at $\lambda = 671$ nm within the frequency interval $\Delta\omega = 2\pi \times 12.7$ MHz.

For the relative visibility, the agreement between our model and experiment data is very good. Our model captures the correct trend of $\mathcal{L}(I)$.

The curves show a strong nonlinear behavior which is related to the exponential relation between $\gamma_{\rm exc}(T)$ and the temperature T. In Fig. 6 we plot the relative visibility as a function of $D\gamma_{\rm exc}t_{\rm int}$, with $\gamma_{\rm exc}$ defined in Eq. (3).

As shown in Eq. (4), we can link $D\gamma_{\rm exc}$ to the photon number density $D\rho_N$ of the blackbody radiation emitted at 671 nm ($^2P \rightarrow {}^2S$ of Li). The natural choice of the frequency interval of interest $\Delta\omega$ for a Li atom at rest would be the linewidth of the D line, $2\pi \times 5.9$ MHz. However, the atoms are moving in the z direction with a velocity distribution given by Eq. (10). We calculate the Doppler broadening effect and estimate the effective frequency interval $\Delta\omega = 2\pi \times 12.7$ MHz. The upper x axis in Fig. 6 shows the photon density $D\rho_N(T)$.

VI. CONCLUSION

We observed decoherence during the propagation of a lithium atom wave by its interaction with the broadband thermal light radiation emitted by tungsten-halogen lamps. The microscopic decoherence process is due to the transfer of random photon momenta to the atom.

The atom excitation must be achieved inside an atom interferometer so that we can detect the decoherence effect, leading to contradictory requirements: a large radiation temperature and a large atom radiation interaction time must be produced in order to ensure a non-negligible excitation probability of the atoms without perturbing the very sensitive alignment of the atom interferometer. Thanks to a photon-recycling box, we succeeded, but its poor efficiency limited the observed decoherence effect, with a reduction of the fringe visibility not larger than ∼22%, while we had predicted a reduction larger than 48% with the expected box efficiency.

We developed a model related to our experimental setup. For an n absorption-emission cycle we derived the probabilities to detect the atom, and with the probabilities of an n absorption-emission cycle, we derived the fringe visibility and mean intensity. Using a single fit parameter, this model is used to fit experimental results; the agreement for the fringe visibility is very good, and for the mean intensity it is satisfactory.

TABLE II. For each atom, we give the energy of the first resonance line $\hbar\omega_0/k_B$, the excited-state lifetime τ, and the excitation lifetime $t_{\rm exc}$ in the light of the Sun on Earth's orbit.

Atom	$\hbar\omega_0/k_B$(K)	τ(ns)	$t_{\rm exc}$(s)
Li	21442	27	67×10^{-3}
Na	24428	16	67×10^{-3}
Rb	18446	27	40×10^{-3}
Sr	20943	23	52×10^{-3}
Cs	31210	23	35×10^{-3}

The discussion of previous experiments using coherent radiation was based on the idea of Heisenberg's microscope Gedankenexperiment [22,23]. The atom is scattered by a photon which can be detected. However, our employed radiation field is isotropic and chaotic. A scattered photon is embedded in the blackbody radiation, and at 2300 K, we estimated the contribution of a scattered photon to the Heisenberg detection unit to be less than 1%.

With the presence of blackbody radiation being ubiquitous, it should be considered for ultrasensitive atom-interferometer projects. Decoherence in an interferometer decreases the fringe visibility and thus the phase sensitivity. Decoherence by interaction of atoms with radiation is a universal process, with a coherence lifetime of the order of the excitation time $t_{\rm exc} = 1/\gamma_{\rm exc}$. In the case of blackbody radiation at temperature T, this time depends a lot on the atom species because of the frequency of its first resonance transition, on the temperature T, and on the dilution factor.

As an example, we consider an atom interferometer in space, close to Earth's orbit, and the decoherence due to sunlight, with an effective surface temperature of the Sun $T \approx 5800$ K. The atom receives the blackbody radiation emitted within the solid angle of the Sun seen from Earth, $\Delta\Omega$. Taking only this geometric effect, the dilution factor is $D = \Delta\Omega/(4\pi) \approx 5.4 \times 10^{-6}$. We calculated $t_{\rm exc}$ for lithium, sodium, rubidium, strontium, and cesium (see Table II). In all cases, the coherence lifetime is of the order of 5×10^{-2} s. We did not take into account the shielding of the Sun's radiation by Fraunhofer dark lines: this effect is considerable for sodium, with a transmission of ∼5% [27], but negligible for rubidium and strontium, with a transmission of ∼95% [28].

For projected experiments of large atom interferometers in space, an efficient shielding of sunlight will be necessary, as discussed by Dimopoulos *et al.* [29,30].

ACKNOWLEDGMENTS

Many thanks to the technical and administrative staffs of our laboratory for their help. The authors are also thankful to J. Gillot for his role in early stages of this experiment and to J. Aboudarham for his help. Financial support from the CNRS INP, Université Toulouse III – Paul Sabatier, ANR (Grant No.

TABLE III. Values used for the calculation of the probabilities. P_n is the probability for $n = 0, 1$ photon scattering, given by the Poisson equation.

Quantity	Value
$\Delta\nu$	5.7 MHz
v_{Li}	1055 m s^{-1}
Ω_D	$4\,\pi/10$
w_{Li}	30 μm
Δt	9.5 μs
ΔA	3×10^{-7} m^2
λ	671 nm
T	2300 K
$\overline{n}_{\mathrm{BB}}$	8086.6 photons
γ_{exc}	9894 s^{-1}
$P_0(\gamma_{\mathrm{exc}}\Delta t)$	0.91
$P_1(\gamma_{\mathrm{exc}}\Delta t)$	0.09

ANR-11-BS04-016-01 HIPATI), and Région Midi-Pyrénées is gratefully acknowledged.

APPENDIX A: A SIMPLE ANALYZE OF THE PHOTON SIGNAL FOR A HYPOTHETICAL HEISENBERG MICROSCOPE IN THE PRESENCE OF BLACKBODY RADIATION

Let us consider that a photon-counting detection unit is placed above one interferometer arm. This unit has an acceptation solid angle of Ω_D, and as we assume isotropic emission, the probability of a scattered photon to be detected is $\Omega_D/4\pi$. The scattering probability is given by $P_1(\gamma_{\mathrm{exc}}\Delta t)$, with P_n being the Poisson distribution, γ_{exc} given by Eq. (5), and Δt being the observation time.

We now consider the effect of blackbody radiation on one photon detector. The mean number of photons $\overline{n}_{\mathrm{BB}}$ is given by

$$\overline{n}_{\mathrm{BB}}(\Omega_D) = \frac{2\nu^2}{c^2}\left\{\exp\left[\left(\frac{h\nu}{k_B T}\right) - 1\right]\right\}^{-1} \Delta\nu\,\Delta A\,\Omega_D\,\Delta t. \tag{A1}$$

We assume that only photons with $\Delta\nu$, the natural linewidth of the $^2S_{1/2} \rightarrow {}^2P$ transition, are detected. The detector is sensitive to blackbody photons coming from an area ΔA and detection angle Ω_D. We define the emission area $\Delta A = w_{\mathrm{Li}} v_{\mathrm{Li}} \Delta t$, with w_{Li} being the width of each interferometer arm's beams and v_{Li} being the atom velocity. Table III summarizes the used quantities.

The probability to detect n photons from the blackbody radiation is governed by the Poisson distribution. For an n-photon event of the detection unit, three contributions exist.

(i) No scattering occurs. The probability is

$$P_n^{(\mathrm{nsc})} = P_0(\gamma_{\mathrm{exc}}\Delta t) P_n(\overline{n}_{\mathrm{BB}}).$$

(ii) A photon is scattered into the detection solid angle; i.e., it is detected:

$$P_n^{(\mathrm{sc,d})} = \frac{\Omega_D}{4\pi} P_1(\gamma_{\mathrm{exc}}\Delta t) P_{n-1}(\overline{n}_{\mathrm{BB}}).$$

TABLE IV. $\overline{n}_{\mathrm{BB}}$ and $P_{n+1}^{(\mathrm{sc,d:rel.})}$ as a function of T.

T (K)	2300	1200	1000	770
$\overline{n}_{\mathrm{BB}}$	8086.6	1.6	0.0	0.0
n_c	8088	3	1	1
$P_{n_c}^{(\mathrm{sc,d:rel.})}$ (%)	0.9	1.6	16.4	99.2

(iii) A photon is scattered into the complementary solid angle; it does not contribute to detection:

$$P_n^{(\mathrm{sc,nd})} = \left(1 - \frac{\Omega_D}{4\pi}\right) P_1(\gamma_{\mathrm{exc}}\Delta t) P_n(\overline{n}_{\mathrm{BB}}).$$

The relative probability to scatter one photon which contributes to detection is

$$P_n^{(\mathrm{sc,d:rel.})} = \frac{P_n^{(\mathrm{sc,d})}}{P_n^{(\mathrm{nsc})} + P_n^{(\mathrm{sc,nd})} + P_n^{(\mathrm{sc,d})}}. \tag{A2}$$

We consider counting events of $n_c = \overline{n}_{\mathrm{BB}} + 1$, and we calculate $P_{n_c}^{(\mathrm{sc,d:rel.})}$ (Table IV). For $T = 2300$ K, $P_{n_c}^{(\mathrm{sc,d:rel.})}$ is small, about 1%. In order to study the effect of temperature on the signal, we keep γ_{exc} constant, but we reduce the temperature of the emitting area ΔA. As expected, $P_{n_c}^{(\mathrm{sc,d:rel.})}$ increases for lower temperatures. Below 770 K, it is larger than 99%. This is due to the rapid decrease in photon flux emitted by blackbody radiation at 671 nm.

APPENDIX B: THE SPECTRAL ENERGY DENSITY IN THE BOX

Assuming a stationary state, the radiation energy produced is equal to the radiation energy either absorbed by the box's internal surfaces or lost by the holes. Each surface, labeled by the index i, is characterized by its area S_i, its emissivity $\varepsilon_i(\omega)$, and its temperature T_i: we take into account the lamp filaments $i = f$, the box's internal surface $i = b$, the holes $i = h$, and the light-absorbing surfaces $i = a$ in the lamps and in the feedthroughs. We consider these last two surfaces to be fully absorbing, with $\varepsilon_h = \varepsilon_a = 1$. As we are interested in the energy density at the wavelength λ_r, the lamp filaments are the only surfaces hot enough to emit at this wavelength.

The balance of the emitted and absorbed radiation energies gives the value of the dilution factor $D(\omega)$, which measures the density of the radiation energy as a fraction of the blackbody radiation energy at the filament temperature T_f:

$$D(\omega) = \frac{\varepsilon_f(\omega) S_f}{\varepsilon_f(\omega) S_f + \varepsilon_b(\omega) S_b + \varepsilon_h S_h + \varepsilon_a S_a}. \tag{B1}$$

To get a rough estimate of $\varepsilon_f S_f$ for the ensemble of the two lamps, we assume that the nominal lamp power, 250 W, is equal to the emitted power, with the filament temperature T_f taken to be equal to the nominal color temperature 3200 K: we thus get $\varepsilon_f S_f \approx 0.84$ cm^2. The box internal surface area is $S_b \approx 105$ cm^2, and the calculated silver emissivity is $\varepsilon_b(\omega_r) = 0.009$ for ω_r. The hole total area is $S_h \approx 1$ cm^2, and we estimate the total absorbing area $S_a \approx 2$ cm^2. With these figures, we get $D(\omega_r) \approx 0.18$.

Unfortunately, a soot layer produced by UV cracking of the Santovac oil used in the diffusion pumps reduced the box efficiency by increasing $\varepsilon_b(\omega_r)$ to an unknown value. As a

consequence, our calculation of $D(\omega_r)$ is not valid, and $D(\omega_r)$ will be fitted by the experimental results.

APPENDIX C: THE LAMP FILAMENT TEMPERATURE

We want to know the radiation density for the resonance frequency of lithium ω_r as a function of the current I in the lamps. We use an energy balance equation to evaluate the filament temperature T_f as a function of the current I. This technique was used in Ref. [31], which showed that, when the filament temperature is large, $T_f > 2000$ K, the power lost by radiation largely dominates the power lost by heat conduction. With this approximation, the power produced by the Joule effect is equal to the power lost by radiation:

$$R(T_f)I^2 = \varepsilon(T_f)S_f\sigma T_f^4. \tag{C1}$$

$R(T_f)$ is the resistance of the filament, I is the current in the lamp, $\varepsilon(T_f)$ is the total emissivity of tungsten, S_f is the emitting surface of the filament, and σ is the Stefan-Boltzmann constant $\sigma = 5.67 \times 10^{-8}$ W m^{-2} K^{-4}.

For $R(T_f)$, we use the equation given by Ref. [31]:

$$R(T_f)/R(300) = -0.5243 + 4.6613 \times 10^{-3}T_f + 2.842 \times 10^{-7}T_f^2, \tag{C2}$$

and for $\varepsilon(T_f)$, we fit the CRC handbook data [32] over the range 2000–3600 K,

$$\varepsilon(T_f) = -3.95 \times 10^{-2} + 2.013 \times 10^{-3}T_f - 2.56 \times 10^{-7}T_f^2. \tag{C3}$$

To determine the ratio $S_f/R(300)$ for the lamps (OSRAM model 64655 HLX), we assume that the filament temperature T_f is equal to the color temperature, 3200 K, when the lamp is operated with its nominal power of 250 W. We thus get $S_f/R(300) = 9.225 \times 10^{-4}$ m$^2/\Omega$. We can then use Eq. (C1) to calculate the temperature T_f (in degrees Kelvin) as a function of the current I (in amperes). We use a fit to invert the relation, and we get

$$T_f = 765.6 \times I^{0.611}. \tag{C4}$$

This formula predicts that the tungsten melting temperature, 3695 K, is reached for a current $I \approx 13.1$ A, while we observe melting of the filament for a current near 12.5 A corresponding to $T_f \approx 3580$ K. However, Eq. (C4) gives an average temperature, whereas the central part of the filament is hotter because it intercepts more radiation than the end parts: a rough estimate of this effect predicts a temperature difference ~150 K, which has the right order of magnitude to explain this discrepancy.

APPENDIX D: EFFECT OF THE MAGNETIC-FIELD GRADIENT DUE TO THE CURRENT CIRCULATING IN THE LAMPS

The interferometer signal is the sum of the contributions of the eight hyperfine Zeeman sublevels F, m_F of the ground state of a ^{7}Li atom (ground state $^2S_{1/2}$ with a nuclear spin $I = 3/2$).

In the presence of a gradient of the magnetic-field modulus B, the phases of the fringe signals due to these sublevels are different, and the fringe visibility $\mathcal{V}$ is reduced [33,34]:

$$\frac{\mathcal{V}}{\mathcal{V}_0} = \frac{1}{4}\{(1+\chi)[1+2\cos(J_{1/2})] + (1-3\chi)\cos(J_1)\} \approx 1 - \frac{J_1^2}{16}(3-5\chi), \tag{D1}$$

where the approximate form is valid if $J_1 \ll 1$ rad. J_1 is given by

$$J_1 = \frac{\mu_B}{\hbar v}\int_{z_{\min}}^{z_{\max}} \frac{\partial B}{\partial x}\delta x(z)dz, \tag{D2}$$

where $\delta x(z)$ is the distance between the interferometer arms, $\delta x(z) = 2\theta_B(z_{M_3} - z)$. $z_{\min}$ and $z_{\max}$ are the z coordinates of the two ends of the interaction region. Finally, χ measures the population imbalance of the two hyperfine sublevels in the atom-interferometer signal [34], and by definition, χ verifies $-1/5 \leqslant \chi \leqslant 1/3$.

The magnetic field $\mathbf{B}$ is the sum of the laboratory magnetic field $\mathbf{B}_{\text{lab}}$, which has a negligible gradient, and the magnetic field $\mathbf{B}_w$ produced by the current in the lamp wire. The laboratory magnetic field $\mathbf{B}_{\text{lab}}$ is Earth's field, perturbed by the steel support of the vacuum tank: its largest component is vertical, along the y axis, with $B_{\text{lab},y} \approx 4 \times 10^{-5}$ T.

The magnetic field $\mathbf{B}_w$ is due to two parallel wires fixed on the vertical side of the photon box at midheight: they carry the current to the lamp which is farthest from mirror M_3 (see Fig. 7). The wires carrying the current to the lamp closest to mirror M_3 produce a similar magnetic field gradient, but this gradient is applied a small distance from $z_{\max}$ and z_{M_3}, and $\delta x(z) = 2\theta_B(z - z_{M_3})$ is very small: the contribution to the integral J_1 associated with the lamp closest to mirror M_3 is considerably smaller than the contribution associated with the lamp farthest from mirror M_3.

The components of the magnetic field $\mathbf{B}_w$ field are given by

$$B_{w,x} = \frac{\mu_0 I}{\pi}\frac{y_w}{(x-x_w)^2 + y_w^2}, \quad B_{w,y} = 0, \quad B_{w,z} = 0, \tag{D3}$$

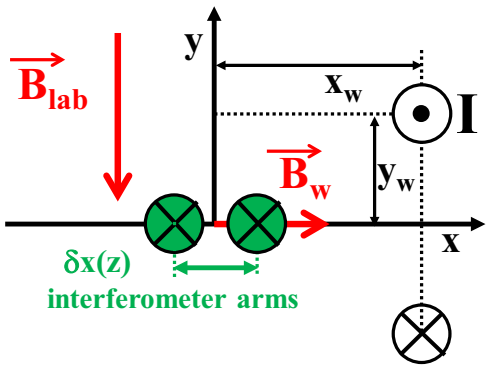

FIG. 7. The $x - y$ plane of the photon box (not to scale), situated between $z_{\min}$ and $z_{\max}$. The wires for the lamp closest to the detector are oriented in the z direction and carry a current I. They are situated at $x_w = 16$ mm and $y_w = \pm 1$ mm.

where the wires are approximated as being infinite in the z direction. The gradient $\partial B/\partial x$ of the magnetic field modulus B is given by

$$\frac{\partial B}{\partial x} \approx 2\frac{B_{w,x}^2}{B}\frac{x - x_w}{(x - x_w)^2 + y_w^2}.$$

For the largest current $I = 12\,\mathrm{A}$, we calculate $B_{w,x} = 1.9 \times 10^{-5}\,\mathrm{T}$ in the region of the two interferometer arms ($x = 0$), which is comparable to the laboratory magnetic field. In this region we get $\partial B/(\partial x) = 9.8 \times 10^{-4}\,\mathrm{T/m}$. Then, using $v = 1055\,\mathrm{ms}^{-1}$, $z_{M_3} - z_{\min} = 130$ mm, and $z_{M_3} - z_{\max} = 30$ mm, we obtain $J_1 = 0.11$ rad. For a balanced hyperfine population i.e., $\chi = 0$, we find $\mathcal{V}/\mathcal{V}_0 = 0.998$, with comparable values for any χ value. As a consequence, the visibility reduction due to the magnetic-field gradient is fully negligible in our experiment.

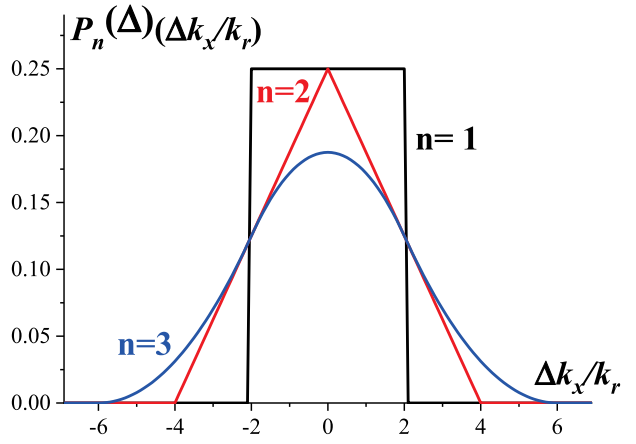

FIG. 8. Probability function $P_n^{(\Delta)}$ as a function of $\Delta k_x/k_r$. We use a solid black line for $n = 1$, a solid red line for $n = 2$, and a solid blue line for $n = 3$.

APPENDIX E: INELASTIC DIFFUSION

After photon absorption followed by a spontaneous emission, an atom has a large probability of being transferred to a different hyperfine Zeeman sublevel F, m_F of its ground state. Pritchard and his coworkers ruled out this effect in their decoherence studies with their sodium interferometer [11,12]: it was obtained by pumping the sodium atoms in the $F = 2, m_F = 2$ ground sublevel and by exciting a cycling transition toward the $F' = 3, m_F = 3$ excited sublevel. The use of a cycling transition was absolutely necessary in the experiment testing the decoherence by multiple excitations [12].

In our experiment, as the blackbody radiation is unpolarized and almost isotropic, the transfer from one hyperfine Zeeman sublevel F_1, m_{F_1} to another one F_2, m_{F_2} occurs with a high probability. However, if the magnetic field B is homogeneous over the interferometer arms, the random phase shift associated with this transfer is negligible.

This phase shift $\delta\varphi$ is due to the fact that the excitation of the two arms does not occur at the same value of the z coordinate: to evaluate this difference δz, we must consider that the excitation can be done by any plane wave with a wave vector k making an angle θ with the z axis. As a consequence, δz is a random quantity, equal to $\delta z = \delta x(z)/\sin\theta$, where $\delta x(z)$ is the distance between the interferometer arms. The resultant phase shift $\delta\varphi$ is given by

$$\delta\varphi = (g_{F_1} m_{F_1} - g_{F_2} m_{F_2})\mu_B B\frac{\delta z}{\hbar v}, \tag{E1}$$

where g_{F_i} is the Landé factor of the hyperfine level F_i. As the order of magnitude of δz is the same as that of $\delta x(z)$ and as $\delta x(z)$ is no larger than 15 μm in the interaction volume, the interaction time $\delta z/v$ is of the order of 15 ns, and the value of $\mu_B B\delta z/(\hbar v)$ is 8×10^{-3} rad for the field in the interferometer, close to Earth's magnetic field $B = 4 \times 10^{-5}$ T. The divergence due to the denominator $\sin\theta$ in δz concerns only a very minor fraction of the plane-wave phase space, those waves which propagate parallel to the atom trajectories, and these plane waves are not present because of the photon box's entrance and exit slits.

Finally, the probability of excitation by blackbody radiation is independent of the ground-state sublevel, and the transfer from one sublevel to another one does not modify the probability of successive excitations.

APPENDIX F: THE PROBABILITY DENSITY FUNCTION $P_n^{(\Delta)}(\Delta k_x)$

The probability density function $P_n^{(\Delta)}(\Delta k_x)$ can be derived in the following way. We assume that for photon absorption and emission no privileged direction in space exists. Therefore, $P_1^{(\Delta)}$ is given by a normalized step function, centered at zero:

$$P_1^{(\Delta)} = \frac{1}{4k_r}[H(\Delta k_x + 2k_r) - H(\Delta k_x - 2k_r)]. \tag{F1}$$

H is the Heaviside function. The n-cycle distribution is given by n independent one-step processes obeying an iterative formula:

$$P_n^{(\Delta)}(\Delta k_x) = \frac{1}{4k_r}\int_{-\infty}^{\infty} P_n^{(\Delta)}(\Delta k_x')P_1^{(\Delta)(\Delta k_x - \Delta k_x')}d\Delta k_x', \tag{F2}$$

with $2\pi/k_r \approx 671$ nm being the momentum of the absorbed or emitted photon. Direct induction allows us to prove that

$$P_n^{(\Delta)}(\Delta k_x) = \sum_{k=0}^{n}\frac{(-1)^k}{(4k_L)^n(n-1)!}\binom{n}{k}[\Delta k_x + 2k_r(n-2k)]^{n-1} \times H[\Delta k_x + 2k_r(n-2k)]. \tag{F3}$$

The induction step requires only the use of Pascal's triangle formula as well as index relabeling. Figure 8 shows $P_n^{(\Delta)}$ for $n = 1, 2, 3$ as a function of $\Delta k_x/k_r$. Note that $P_1^{(\Delta)}$ is uniform for $-2k_r \leqslant \Delta k_x \leqslant 2k_r$, which reflects the homogeneity of the absorption and emission directions.

[1] D. Pritchard, Ann. Phys. (Berlin, Ger.) **513**, 35 (2001).
[2] W. H. Zurek, Rev. Mod. Phys. **75**, 715 (2003).
[3] C. J. Myatt, B. E. King, Q. A. Turchette, C. A. Sackett, D. Kielpinski, W. M. Itano, C. Monroe, and D. J. Wineland, Nature (London) **403**, 269 (2000).
[4] Q. A. Turchette, C. J. Myatt, B. E. King, C. A. Sackett, D. Kielpinski, W. M. Itano, C. Monroe, and D. J. Wineland, Phys. Rev. A **62**, 053807 (2000).
[5] M. Brune, E. Hagley, J. Dreyer, X. Maître, A. Maali, C. Wunderlich, J. M. Raimond, and S. Haroche, Phys. Rev. Lett. **77**, 4887 (1996).
[6] S. Haroche, Rev. Mod. Phys. **85**, 1083 (2013).
[7] D. J. Wineland, Rev. Mod. Phys. **85**, 1103 (2013).
[8] T. Pfau, S. Spalter, C. Kurtsiefer, C. R. Ekstrom, and J. Mlynek, Phys. Rev. Lett. **73**, 1223 (1994).
[9] J. F. Clauser and S. Li, Phys. Rev. A **50**, 2430 (1994).
[10] U. Sterr, K. Sengstock, J. H. Müller, D. Bettermann, and W. Ertmer, Appl. Phys. B **54**, 341 (1992).
[11] M. S. Chapman, T. D. Hammond, A. Lenef, J. Schmiedmayer, R. A. Rubenstein, E. Smith, and D. E. Pritchard, Phys. Rev. Lett. **75**, 3783 (1995).
[12] D. A. Kokorowski, A. D. Cronin, T. D. Roberts, and D. E. Pritchard, Phys. Rev. Lett. **86**, 2191 (2001).
[13] L. Hackermüller, K. Hornberger, B. Brezger, A. Zeilinger, and M. Arndt, Nature (London) **427**, 711 (2004).
[14] H. Uys, J. D. Perreault, and A. D. Cronin, Phys. Rev. Lett. **95**, 150403 (2005).
[15] L. Hackermüller, K. Hornberger, B. Brezger, A. Zeilinger, and M. Arndt, Appl. Phys. B **77**, 781 (2003).
[16] K. Hornberger, S. Uttenthaler, B. Brezger, L. Hackermuller, M. Arndt, and A. Zeilinger, Phys. Rev. Lett. **90**, 160401 (2003).
[17] J. Schmiedmayer, M. S. Chapman, C. R. Ekstrom, T. D. Hammond, D. A. Kokorowski, A. Lenef, R. A. Rubinstein, E. T. Smith, and D. E. Pritchard, in *Atom Interferometry*, edited by P. R. Berman (Academic Press, San Diego, 1997), p. 1.
[18] M. Safronova, D. Jiang, B. Arora, C. Clark, M. Kozlov, U. Safronova, and W. Johnson, IEEE Trans. Ultrason. Ferroelectr. Freq. Control **57**, 94 (2010).
[19] M. Sonnleitner, M. Ritsch-Marte, and H. Ritsch, Phys. Rev. Lett. **111**, 023601 (2013).
[20] P. Haslinger, M. Jaffe, V. Xu, O. Schwartz, M. Sonnleitner, M. Ritsch-Marte, H. Ritsch, and H. Müller, Nat. Phys. **14**, 257 (2018).
[21] B. Canuel *et al.*, Class. Quantum Grav. **37**, 225017 (2020).
[22] W. Heisenberg, Z. Phys. **43**, 172 (1927).
[23] R. Feynman, R. Leighton, and M. Sands, *The Feynman Lectures on Physics* (Addison-Wesley, Reading, MA, 1965), Vol. 3, pp. 5–7.
[24] A. Miffre, M. Jacquey, M. Büchner, G. Trénec, and J. Vigué, Eur. Phys. J. D **33**, 99 (2005).
[25] K. Hornberger, J. E. Sipe, and M. Arndt, Theory of decoherence in a matter-wave Talbot-Lau interferometer, Phys. Rev. A **70**, 053608 (2004).
[26] B. Décamps, J. Gillot, A. Gauguet, J. Vigué, and M. Büchner, Eur. Phys. J. D **71**, 334 (2017).
[27] D. P. McNutt and J. E. Mack, J. Geophys. Res. **68**, 3419 (1963).
[28] D. L. Lambert and E. A. Mallia, Mon. Not. R. Astron. Soc. **140**, 13 (1968).
[29] S. Dimopoulos, P. W. Graham, J. Hogan, M. Kasevich, and S. Rajendran, Proc. Int. Sch. Phys. "Enrico Fermi" **188**, 237 (2014).
[30] S. Dimopoulos, P. W. Graham, J. M. Hogan, M. A. Kasevich, and S. Rajendran, in *Proceedings of the International School of Physics "Enrico Fermi"*, edited by G. M. Tino and M. A. Kasevich (2014), Vol. 188.
[31] C. de Izarra, https://hal.science/hal-00445665.
[32] *Handbook of Chemistry and Physics*, 63rd ed. (CRC Press, Boca Raton, FL, 1982–1983).
[33] M. Jacquey, A. Miffre, M. Büchner, G. Trénec, and J. Vigué, Europhys. Lett. **77**, 20007 (2007)
[34] S. Lepoutre, J. Gillot, A. Gauguet, M. Büchner, and J. Vigué, Phys. Rev. A **88**, 043628 (2013).